Applied Physics A (2021) 127:735
https://doi.org/10.1007/s00339-021-04883-1

Applied Physics A
Materials Science & Processing

Performance improvement of planar silicon heterojunction solar cells via sandwich-like p-type emitters

Jiakai Zhou[1,2,3,4] · Boyu Zhang[1,2,3,4] · Junfan Chen[1,2,3,4] · Huizhi Ren[1,2,3,4] · Qian Huang[1,2,3,4] · Xiaodan Zhang[1,2,3,4] · Guofu Hou[1,2,3,4] · Ying Zhao[1,2,3,4]

Received: 2 July 2021 / Accepted: 26 August 2021 / Published online: 4 September 2021

Abstract

The emitter is one of the most crucial issues to achieve high-performance silicon heterojunction (SHJ) solar cells. In this work, we study the effects of single-layer and multi-layer p-type emitters, including boron-doped hydrogenated nanocrystalline silicon (nc-Si:H) and/or boron-doped hydrogenated nanocrystalline silicon oxide (nc-SiO_X:H) films, on the device performance of SHJ solar cells. The results demonstrate that the sandwich-like p-type emitters of p-nc-Si:H/p-nc-SiO_X:H/p^+-nc-Si:H have the potential to become an effective and efficient candidate to result in higher efficiency. The lightly boron-doped p-nc-Si:H is used to reduce the incubation layer thickness in the initial stage of growth, while the low parasitic absorption of the p-nc-SiO_X:H emitter leads to an increase in short-circuit current. Moreover, a highly boron-doped p^+-nc-Si:H layer is implemented on top of the p-nc-SiO_X:H to get a lower series resistance (R_s) and higher fill factor. Lastly, we achieve a champion SHJ solar cell on planar wafer with an open-circuit voltage of 678.2 mV, a short-circuit current density of 36.6 mA/cm^2, a fill factor of 77% and a conversion efficiency of 19.11%.

Graphic abstract

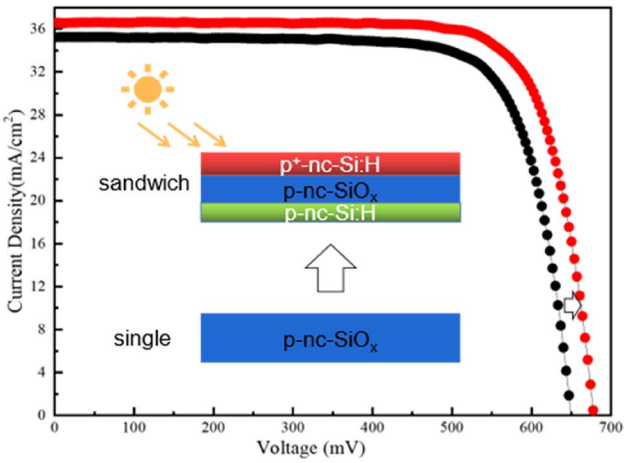

Keywords Silicon heterojunction · Solar cells · Planar wafer · p-type emitters · Triple layers

1 Introduction

The silicon heterojunction (SHJ) solar cell is considered as one of the most promising candidates for the next-generation high-efficiency crystalline silicon (c-Si) device [1]. Although the interdigitated back contact silicon heterojunction

✉ Guofu Hou
gfhou@nankai.edu.cn

Extended author information available on the last page of the article

(IBC-SHJ) architecture resulted in the world-record efficiency of 26.63%, the both side-contacted SHJ architecture is still the popular candidate because of its relatively simple processes [2, 3]. However, the champion efficiency of 25.11% for the both side-contacted SHJ solar cell is lower than that of 25.8% for the homojunction c-Si solar cell with the so-called tunnel oxide passivating contact (TOPCon) structure, which is mainly attributed to the relatively lower short-circuit current density (J_{SC}) [4–9]. Usually, it is easy to get J_{SC} values around 42 mA/cm^2 for the both side-contacted homojunction c-Si solar cells, while the typical J_{SC} values for the both side-contacted SHJ solar cells are in the range from 39 to 40 mA/cm^2, which are notably caused by the parasitic absorption of window layers [10–13]. Therefore, in addition to applying as thin as possible a window layer, an alternative approach is to alloy hydrogenated silicon films with oxygen or carbon to get wider bandgap and lower parasitic absorption [14–17]. Another necessary characteristic for the window layers is high conductivity to get a lower series resistance between the emitter/ITO contact, which is benefit for the fill factor (*FF*) and open-circuit voltage (V_{OC}) [15, 18–21]. Thus, hydrogenated silicon alloys with nanometer crystals embedded in amorphous silicon matrix were proposed, in which nanocrystals not only result in high conductivity but also help to increase the bandgap because of quantum confinement effect [14, 22–24]. Due to its tunable refractive index, a low absorption coefficient and a sufficient electrical conductivity, recently considerable works have proved the effectiveness of hydrogenated nanocrystalline silicon oxide (nc-SiO_X:H) films as the window/emitter layers in the both side-contacted SHJ solar cells [25–27]. For example, the record efficiency of 25.11% has been obtained using hydrogenated microcrystalline silicon oxide as the front surface field to get high enough J_{SC} value [4].

For the SHJ solar cell, an intrinsic a-Si:H layer is the crucial and indispensable part to get better c-Si surface passivation and then higher efficiency [17, 28, 29]. However, it is a very challenging issue to nucleate and then form highly crystalline layers on an a-Si:H passivation layer, which will be even more difficult since the window layer is only 15 nm or less in the SHJ solar cell [30]. In addition, although the introduction of oxygen or carbon increases light transmission, it is inevitable to further reduce the crystallinity of hydrogenated nanocrystaline silicon alloy films. Various interface treatment methods have been developed to realize fast nucleation on the a-Si:H layers while maintaining excellent passivation quality [31]. The first and the most popular method is hydrogen plasma treatment (HPT) on the (i)a-Si:H/c-Si interface, which can result in high chemical interface-passivation quality and help to the nucleation and crystallinity of following hydrogenated nanocrystaline silicon alloys layer [32, 33]. An alternate CO_2 plasma treatment was also proved to get similar results [34–37]. Another efficient method is to deposit an ultra-thin, highly crystalline seed layer to inhibit the amorphous incubation layer and form a nucleation layer to improve the crystallinity [38, 39].

From above analysis, we can find that for the emitters of silicon heterojunction (SHJ) solar cells, which simultaneously act as the window layers, high conductivity and wide bandgap are essential parameters to achieve effective carrier transportation and collection and then the total device performance. In this study, various p-type emitters including single-, double- and sandwich-like triple layers were designed by combination of boron-doped nanocrystaline silicon (p-nc-Si:H) and boron-doped nanocrystaline silicon oxide (p-nc-SiO_X:H) layers [40]. The aim is to take advantage of both the high crystallinity, better charge carrier transport and low contact resistance of p-nc-Si:H and a much reduced parasitic absorption of p-nc-SiO_X:H. The experimental results indicate that a sandwich-like emitter with p-nc-Si:H/p-nc-SiO_X:H/p$^+$-nc-Si:H triple layers has the potential to become an efficient and effective way to improve the SHJ device performance.

2 Experimental methods

Double-sided polished FZ *n*-type c-Si wafers with < 111 > orientation, thickness of 275 ± 10 μm and electrical resistivity of 2–10 Ω cm were adopted in this study. All the wafers were successively cleaned by acetone, deionized water, ultrasonic cleaning, RCA1 and RCA2 procedures. Then, these wafers were immediately loaded into the Cluster tool plasma enhanced chemical vapor deposition (PECVD) system to deposit the i-a-Si:H passivation layers, p-type emitter layers and n-type layers. All p-nc-Si:H, p-nc-SiO_X:H, and p + -nc-Si:H layers were deposited at 200 ℃ substrate temperature with SiH_4, CO_2, H_2 as process gases and PH_3 or $B(CH_3)_3$ as doping gases. The device configuration of the planar SHJ solar cells in this study was Ag grid/ITO/*p*-type emitter/i-a-Si:H/N-FZ-Si/i-a-Si:H/n-type layer/Al back contact. The ITO layer, Ag grid and Al back contact were deposited by the thermal evaporation.

A Cary 5000 spectrometer was used to measure the transmission and reflection spectra, and the bandgaps of the Si thin film materials were calculated using Tauc formula in conjunction with the test results. A programmable Keithley617 electrometer with high precision was used to test the conductivity. Raman scattering was measured on glass substrates by a Renishaw RM2000 microscope with a 488 nm laser. The current density versus voltage (*J*–*V*) curves were measured by an AM1.5 solar simulator (WXS-156S-L2, AM1.5GMM) with 100 mW/cm^2 at 25 ℃. The external quantum efficiency (EQE) spectra were measured by using a QEX10 PV system, and the J_{SC} was calculated by the integral of measured EQE and the AM1.5 solar spectra.

To measure the passivation quality, Sinton Instruments WCT-120 QSSPC tester was used in transient or quasi-steady state analysis mode of generalized (1/1) or (64/1) at an injection level of $1\times10^{15}/cm^3$.

3 Results and discussion

3.1 Structural and optoelectronic properties of p-type layers

The first step is to study the optoelectronic properties of p-type layers. Five samples named as 1#, 2#, 3#, 4# and 5# represent p^+-nc-Si:H, p-nc-Si:H, p-nc-SiO_X:H, p-nc-Si:H/p-nc-SiO_X:H and p-nc-Si:H/p-nc-SiO_X:H/p^+-nc-Si:H, respectively. All the samples were deposited with the same temperature of 300 ℃, chamber pressure of 1.98 Torr and RF power of 10 W. Other deposition parameters are listed in Table 1. Figure 1 shows the Raman spectra of these five p-type layers. It can be found that for the 1#, 2# and 3# samples, broad amorphous peaks at 480 cm^{-1} were dominated, while only slight signals from 515 to 520 cm^{-1} occur, which indicates that these layers are in the mixed state of amorphous and nanocrystalline grains. From the Raman spectra of 1# and 2# samples, it can be seen that a heavily dopant can cause a slightly reduced crystallinity. The introduction of CO_2 also reduces the crystallinity from the Raman spectra of 1#, 2# and 3# samples. In order to increase the crystallinity, a double-layered sample (4#) is designed with p-nc-Si:H/p-nc-SiO_X:H, of which a slightly doped p-nc-Si:H serve as the seed layer. Since the bandgap of p-nc-Si:H is much lower than that of p-nc-SiO_X:H as shown in Table 1, the seed layer should be as thin as possible to guarantee the light transparence. The Raman spectra show that even only 2 nm seed layer is applied, there still exists a remarkable peak at 520 cm^{-1}, which indicates the much more improved crystallinity compared to the single-layered samples 1#, 2# and 3#. The triple-layered sample (5#) with p-nc-Si:H/p-nc-SiO_X:H/p^+-nc-Si:H also demonstrated similar results.

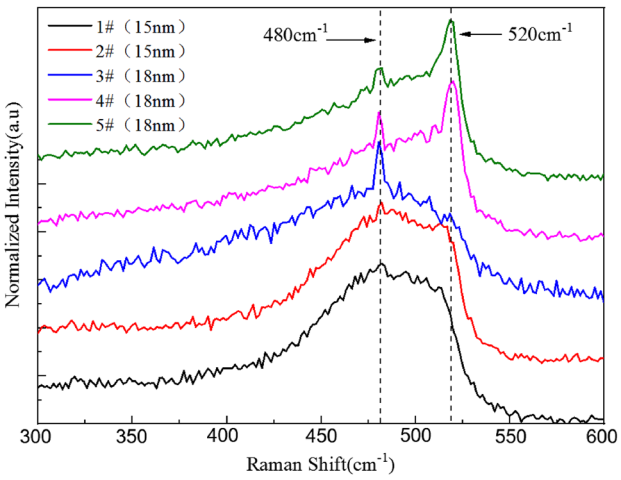

Fig. 1 Raman spectra of different p-type layers on glass substrates. 1# p^+-nc-Si:H, 2# p-nc-Si:H, 3# p-nc-SiO_X:H, 4# p-nc-Si:H/p-nc-SiO_X:H, 5# p-nc-Si:H/p-nc-SiO_X:H/p^+-nc-Si:H

The optical transmittance (T), reflectance (R) spectra of those five p-type layers were measured and the absorbance (1-T-R) result is calculated, as shown in Figure 2. It can be found that the single-layered 1# and 2# samples demonstrate the lowest transmittances. Even though the 3# sample was composed of p-nc-SiO_x:H layer, its transmittance is still lower than those for the double-layered (4#) and triple-layered (5#) samples. The reasons can be partly contributed to the enhanced crystallinity of 4# and 5# samples, which leads to increased oxygen content and different Si–O bonds. In fact, the calculated bandgap (E_g) values for these five samples in Table 1 also prove above explanations. The E_g value of 3# sample is 2.03 eV, which is much higher than those for 1# and 2# samples but much lower than those for 4# and 5# samples.

Table 1 The deposition parameters and optoelectronic properties of p-type layers

Sample No	p-type layers	H_2 (sccm)	SiH_4 (sccm)	TMB (sccm)	CO_2 (sccm)	Thickness (nm)	Conductivity (S/cm)	Bandgap (eV)
1#	p^+-nc-Si:H	400	2	2	–	15	6.25E–3	1.79
2#	p-nc-Si:H	180	1	2.4	–	15	8.94E–5	1.72
3#	p-nc-SiO_X:H	400	0.75	2	0.5	18	7.81E–9	2.07
4#	p-nc-Si:H/p-nc-	180	1	2.4	–	2	1.01E–6	2.28
	SiO_X:H	400	0.75	2	0.5	16		
5#	p-nc-Si:H/p-nc-	180	1	2.4	–	2	7.40E–5	2.29
	SiO_X:H/p^+-nc-	400	0.75	2	0.5	14		
	Si:H	400	2	2	–	2		

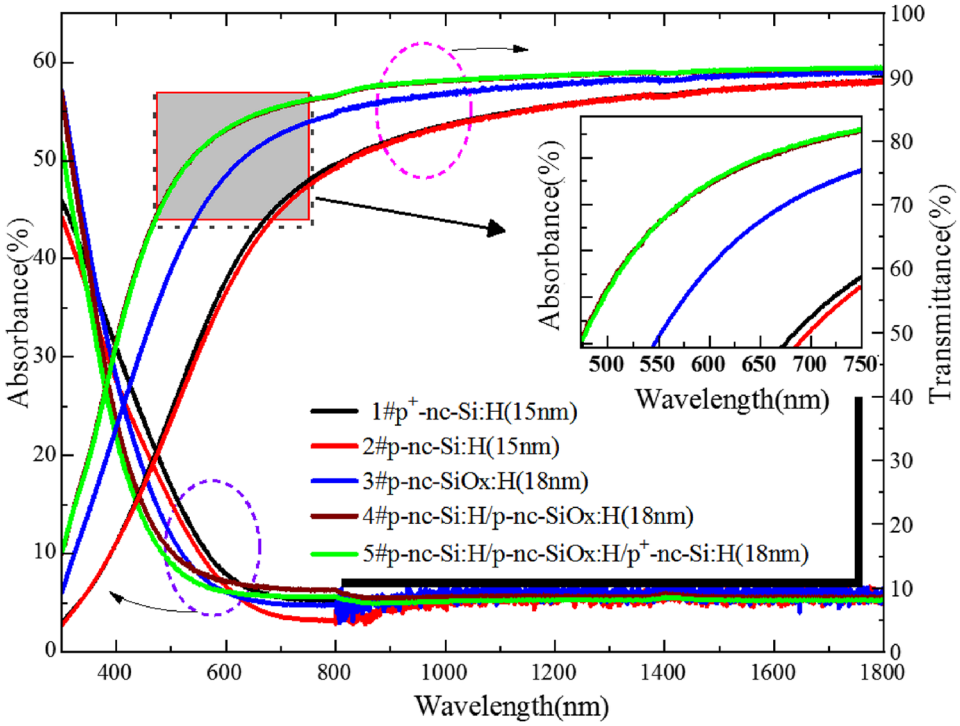

Fig. 2 Transmittance and absorbance of different p-type layers

Conductivities of these five p-type layers are also listed in Table 1. Compared with 1# and 2# sample, a heavily TMB dopant significantly increases the conductivity from 8.94×10^{-5} to 6.25×10^{-3} S/cm. The introduction of CO_2 into the film (3# sample) leads to a dramatic reduction of the conductivity to an as low value as 7.81×10^{-9} S/cm. When the p-nc-Si:H layers were used as seed layers prior to p-nc-SiOx:H layers, the conductivity of 4# sample increases to 1.01×10^{-6} S/cm. If the p + -nc-Si:H layer was used to cover 4# sample, the conductivity of the sandwich-like p-type layer (5# sample) further increases to 7.40×10^{-5} S/cm, which is very close to that of 2# sample. From above design and optimization, we can conclude that high crystallinity, high conductivity and wide bandgap can be simultaneously obtained by the sandwich-like p-type layer (5# sample).

3.2 SHJ solar cells with different *p*-type emitter/window layers

In this section, three p-type layers were adopted as the emitter/window layers in SHJ solar cells. The first type is p-nc-SiOx:H single layer with the same deposition parameters as that of 3# in Table 1, as shown in Figure 3a. The second one consists of a lightly doped p-nc-Si:H layer with low defect density and a low absorption p-nc-SiOx:H layer with the same deposition parameters as that of 4# in Table 1, as shown in Figure 3a. Figure 3c shows the last one named as the sandwich-like emitter with p-nc-Si:H/p-nc-SiOx:H/p^+-nc-Si:H triple layers with the same deposition parameters as

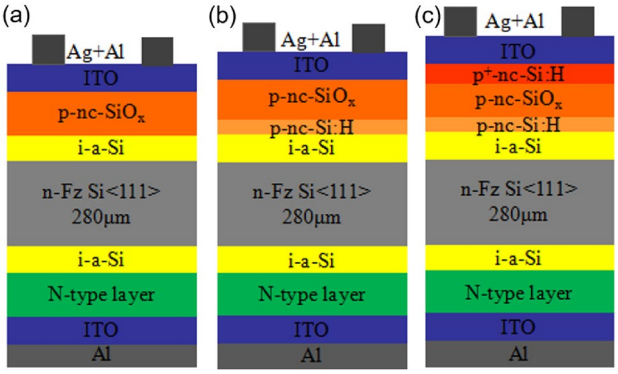

Fig. 3 Schematic diagrams of a-Si:H/c-Si heterojunction solar cells with different p-type emitter/window layers. **a** p-nc-SiO_x:H single layer, **b** p-nc-Si:H/p-nc-SiO_x:H double layers and **c** sandwich-like emitter with p-nc-Si:H/p-nc-SiO_x:H/p^+-nc-Si:H triple layer

that of 5# in Table 1, of which the lightly doped p-nc-Si:H layer with 2 nm act as a seed layer to get a fast nucleation and increase the total crystallinity of the p-emitter/window layer. The low absorption p-nc-SiO_X:H layer with 14 nm leads to a reduced parasitic absorption and improve the J_{SC} of the solar cell. The highly doped p^+-nc-Si:H layer with 2 nm is implemented on top of the sandwich-like emitter to achieve a lower series resistance and improve the p-emitter/TCO contact.

The illuminated *J–V* curves of these SHJ solar cells are shown in Figure 4, while the corresponding external

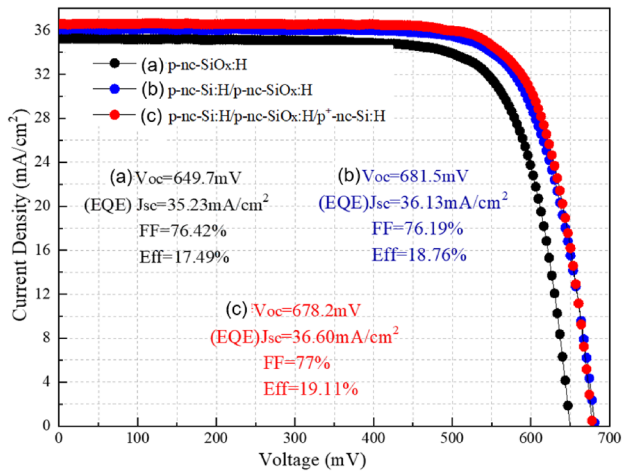

Fig. 4 Illuminated *J–V* curves of SHJ solar cells with different p-type emitter/window layers

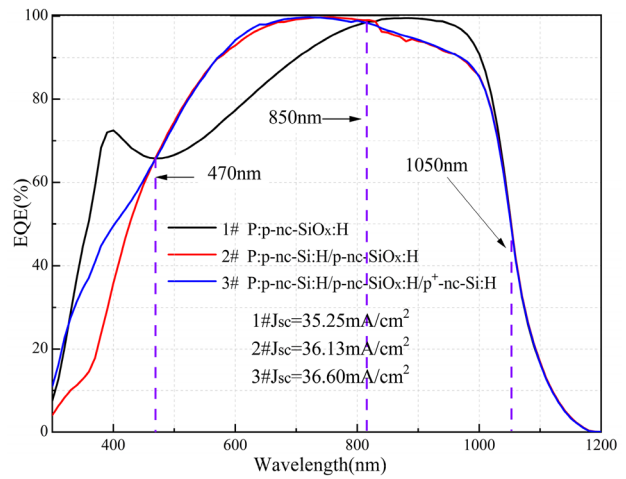

Fig. 5 EQE curves of SHJ solar cells with different p-type emitter/window layers

quantum efficiencies are present in Figure 5. Noted that the champion conversion efficiency of SHJ solar cell using a single layer p-nc-Si:H emitter was only 16.7% in our previous study [41]. Figure 4 shows that the V_{OC} and J_{SC} of (a) sample are significantly higher than those of (b) sample. The reason for the V_{OC} improvement can be contributed to the higher conductivity (as shown in Table 1) by the double-layer p-type emitter/window layer, which benefits to enhance the built-in electric field, reduce the interface carrier recombination and improve the field-effect passivation quality of the solar cell. On the other hand, the high transmittance, wide bandgap and gradient refractive index of the p-nc-Si:H/p-nc-SiO_X:H p-type emitter/window layer help to increase the J_{SC}. When the sandwich-like emitter with p-nc-Si:H/p-nc-SiO_X:H/p^+-nc-Si:H triple layers is adopted, even higher *FF* and J_{SC} are obtained for the (c) sample, which can be explained by the reduced emitter/ITO contact resistance and improved carrier collection because of the improved conductivity of p^+-nc-Si:H layer. A champion efficiency of 19.11% has been achieved with V_{OC} of 678.2 mV, FF of 77% and J_{SC} of 36.6 mA/cm^2 for the planar SHJ cell with an area of 1.0 cm^2. This high-efficiency planar SHJ solar cell can be a very promising candidate as the bottom cell in the perovskite/silicon monolithic tandem solar cell, in which the perovskite top cell is fabricated by a solution procedure [42].

From Figure 5, we can see that these three solar cells demonstrate quite different EQE curves. The solar cell with p-nc-SiO_X:H single layer behaves higher EQE values in the range from 300 to 470 nm and 820 nm to 1050 nm, but a much lower EQE values in the range from 470 to and 820 nm. On the contrany, the solar cells with p-nc-Si:H/p-nc-SiO_X:H double-layer and sandwich-like emitter with p-nc-Si:H/p-nc-SiO_X:H/p^+-nc-Si:H triple layer behave very similar EQE curves. Compared to the solar cell with p-nc-SiO_X:H single layer behaves, they have lower EQE values in the range from 300 to 470 nm and 820 nm to 1050 nm, but a much higher EQE values in the range from 470 to and 820 nm. These phenomena can be partly ascribed to different refractive indexes of these three p-type emitter/window layers. A further optimization of the refractive index gradient of all light-incoming side including ITO, *p*-type emitter/window layer and even a magnesium fluoride (MgF_2) layer with very low refractive index as the anti-reflective coating will be the focus of the next step to improve the spectral response and then the device efficiency. Another necessary emphasis should be to optimize the interface and passivation layer quality to improve the open-circuit voltage, which is still much lower than the state-of-the-art V_{OC} values of SHJ solar cells [13].

4 Conclusions

Various p-type layers by combining p-nc-Si:H, p-nc-SiOx:H and p^+-nc-Si:H layers were proposed and investigated as the emitter/window layer in the planner SHJ solar cell. By studying the structural and optoelectronic properties of various p-type layers and their influence on the SHJ device performance, the novel sandwich-like p-type layer consisting of p-nc-Si:H/p-nc-SiO_X:H/p^+-nc-Si:H triple layers is proved to be the optimal emitter/window layer, which can be contributed to its high crystallinity, high conductivity and wide bandgap. With this novel sandwich-like p-type emitter/window layer, we obtained a V_{OC} of 678.2 mV, a J_{SC} of 36.6 mA/cm^2, a fill factor of 77% and an efficiency of 19.11% on a planar n-type FZ Si-wafer.

Acknowledgements This work was financially supported by the National Key R&D Program of China (Grant No. 2018YFB1500402), The National Natural Science Foundation of China (No. 62074084).

References

1. H. Jan, D. Olivier, B. Mathieu, Sol. Energ. Mat. Sol. C. **187**, 140 (2018)
2. K. Yoshikawa, W. Yoshida, T. Irie, H. Kawasaki, K. Konishi, H. Ishibashi, T. Asatani, D. Adachi, M. Kanematsu, H. Uzu, K. Yamamoto, Sol. Energ. Mat. Sol. C. **173**, 37 (2017)
3. T. Mishima, M. Taguchi, H. Sakata, E. Maruyama, Sol. Energ. Mat. Sol. C. **95**, 1 (2011)
4. X.N. Ru, M.H. Qu, J.Q. Wang, T.Y. Ruan, M. Yang, F.G. Peng, W. Long, K. Zheng, H. Yan, X.X. Xu, Sol. Energ. Mat. Sol. C. **215**, 110643 (2020)
5. A. Richter, J. Benick, F. Feldmann, A. Fell, M. Hermle, S.W. Glunz, Sol. Energ. Mat. Sol. C. **173**, 96 (2017)
6. J. Melskens, B.W.H. Loo, B. Macco, L.E. Black, S. Smit, W.M.M. Kessels, IEEE J. Photovolt. **8**, 373 (2018)
7. S. Zhang, F. Meng, R. Sondena, Z. Liu, G. Tranell, Energy Procedia **124**, 321 (2017)
8. R.V.K. Chavali, S. De Wolf, M.A. Alam, Prog. Photovoltaics **26**, 241 (2018)
9. A.S. Kale, W. Nemeth, S.P. Harvey, M. Page, D.L. Young, S. Agarwal, Sol. Energ. Mat. Sol. C. **185**, 270 (2018)
10. J.H. Bao, K. Tao, Y.R. Lin, R. Jia, A.M. Liu, Chinese Phys. B **28**, 098201 (2019)
11. J.W. Shi, M. Boccard, Z. Holman, Appl. Phys. Lett. **109**, 031601 (2016)
12. F.Y. Meng, L.L. Shen, J.H. Shi, L.P. Zhang, J.N. Liu, Y.C. Liu, Z.X. Liu, Appl. Phys. Lett. **107**, 223901 (2015)
13. M. Taguchi, A. Yano, S. Tohoda, K. Matsuyama, Y. Nakanura, T. Nishiwaki, K. Fujita, E. Maruyama, IEEE J. Photovolt. **4**, 96 (2014)
14. Z.P. Ling, J. Ge, T. Mueller, J. Wong, A.G. Aberle, Energy Procedia **15**, 118 (2012)
15. K.N. Ding, U. Aeberhard, F. Finger, Rau. Phys. Status Solidi-R **6**, 193 (2012)
16. L. Zhao, C.L. Zhou, H.L. Li, H.W. Diao, W.J. Wang, Sol. Energ. Mat. Sol. C. **92**, 673 (2008)
17. H. Yu, R. Cui, H. Wang, H. Yang, B. Zhao, Z. Zhao, D. Tang, S. Lin, J. Mater. Sci. **40**, 1367 (2005)
18. S. Diplas, Thin Solid Films **515**, 8539 (2007)
19. J.S. Christensen, A.G. Ulyashin, K. Maknys, A.Y. Kuznetsov, B.G. Svensson, Thin Solid Films **511**, 93 (2007)
20. K. Ding, U. Aeberhard, F. Finger, U. Rau, J. Appl. Phys. **113**, 134501 (2013)
21. A. Neumuller, O. Sergeev, S.J. Heise, S. Bereznev, O. Volobujeva, J.F.L. Salas, M. Vehse, C. Agert, Nano Energy **43**, 228 (2018)
22. O.M. Ghahfarokhi, K. Von Maydell, C. Agert, Appl. Phys. Lett. **104**, 11 (2014)
23. Y. Lee, H. Kim, S.M. Iftiquar, S. Kim, S. Ahn, Y.J. Lee, V.A. Dao, J. Appl. Phys. **116**, 24 (2014)
24. C. Summonte, R. Rizzoli, D. Iencinella, E. Centurioni, E. Desalvo, A. Zignani, J. Non-Cryst, Solids **338**, 706 (2004)
25. D. Pysch, C. Meinhard, N.P. Harder, M. Hermle, S.W. Glunz, J. Appl. Phys. **110**, 094516 (2011)
26. L. Mazzarella, S. Kirner, B. Stannowski, L. Korte, B. Rech, R. Schlatmann, Appl. Phys. Lett. **106**, 023902 (2015)
27. H. Fujiwara, T. Kaneko, M. Kondo, Appl. Phys. Lett. **91**, 133508 (2007)
28. W.Z. Liu, L.P. Zhang, R.F. Chen, F.Y. Meng, W.W. Guo, J. Bao, Z.X. Liu, J. Appl. Phys. **120**, 671 (2016)
29. W. Wang, E.A. Schiff, Appl. Phys. Lett. **91**, 133504 (2007)
30. F. Feldmann, M. Simon, M. Bivour, C. Reichel, M. Hermle, S.W. Glunz, Appl. Phys. Lett. **104**, 181105 (2014)
31. L. Mazzarella, A.B.M. Vilches, L. Korte, R. Schlatmann, B. Stannowski, Sol. Energ. Mat. Sol. C. **179**, 386 (2018)
32. M.R. Khan, M.A. Alam, Appl. Phys. Lett. **107**, 223502 (2015)
33. A. Descoeudres, L. Barraud, R. Baetlome, G. Choong, D.S. Wolf, F. Zicarelli, C. Ballif, Appl. Phys. Lett. **97**, 183505 (2010)
34. L. Mazzarella, S. Kirner, O. Gabriel, S.S. Schmidt, L. Korte, B. Stannowski, B. Rech, R. Schlatmann, Phys. Status Solidi Appl. Mater. Sci. **214**, 1532958 (2017)
35. L. Mazzarella, S. Kirner, O. Gabriel, L. Korte, B. Stannowski, B. Rech, R. Schlatmann, Energy Procedia **77**, 304 (2015)
36. S. Rattanapan, T. Watahiki, S. Miyajima, M. Konagai, Jpn. J. Appl. Phys. **50**, 082301 (2011)
37. B. Zhang, Y. Zhang, R.D. Cong, Y. Li, W. Yu, G.S. Fu, Sol. Energy **155**, 670 (2017)
38. C. Lei, C.W. Peng, J. Zhong, H.Y. Li, M. Yang, K. Zheng, X.L. Qu, L.L. Wu, C. Yu, Y.M. Li, X.X. Xu, Sol. Energ. Mat. Sol. C. **209**, 110439 (2020)
39. D.P. Pham, S. Kim, S. Lee, A.H.T. Le, E.C. Cho, J. Park, J. Yi, Infrared Phys. Techn. **102**, 103037 (2019)
40. H.B. Huang, G.Y. Tian, T. Wang, C. Gao, J.R. Yuan, Z.H. Yue, L. Zhou, Front. Energy **11**, 92 (2017)
41. J.F. Chen, S.S. Zhao, L.L. Yan, H.Z. Ren, C. Han, D.K. Zhang, C.C. Wei, G.C. Wang, G.F. Hou, Y. Zhao, X.D. Zhang, Chin. Phys. B **29**, 038801 (2020)
42. A. Zouari, A.B. Arab, Renew. Energ. **36**, 1663 (2011)

Authors and Affiliations

Jiakai Zhou[1,2,3,4] · Boyu Zhang[1,2,3,4] · Junfan Chen[1,2,3,4] · Huizhi Ren[1,2,3,4] · Qian Huang[1,2,3,4] · Xiaodan Zhang[1,2,3,4] · Guofu Hou[1,2,3,4] · Ying Zhao[1,2,3,4]

[1] Institute of Photoelectronic Thin Film Devices and Technology of Nankai University, Tianjin 300350, China

[2] Key Laboratory of Photoelectronic Thin Film Devices and Technology of Tianjin, Tianjin 300350, China

[3] Engineering Center of Thin Film Photoelectronic Technology of Ministry of Education, Tianjin 300350, China

[4] Sino-Euro Joint Research Center for Photovoltaic Power Generation of Tianjin, Tianjin 300350, China